IEEE Access
Multidisciplinary | Rapid Review | Open Access Journal

Received 1 February 2024, accepted 23 February 2024, date of publication 18 March 2024, date of current version 26 March 2024.

Digital Object Identifier 10.1109/ACCESS.2024.3378732

RESEARCH ARTICLE

Analysis of EEG Signals Fused With CNN and Complex Networks

LU MA[1] AND HAIPENG XU[2,3]

[1]School of Information and Control Engineering, China University of Mining and Technology, Xuzhou 221116, China
[2]Shangqiu City Development Investment Group Company Ltd., Shangqiu 476000, China
[3]Graduate School, University of the East, Manila 1008, Philippines

Corresponding author: Lu Ma (malu2023@126.com)

ABSTRACT Currently, brain-computer interface technology still poses hidden dangers in the complete control of ideas. Additionally, there are issues with the low sampling frequency and accuracy of EEG signal acquisition equipment. To address these concerns, this study proposes a combined model for EEG signal recognition and classification analysis by combining frequency division multi-feature complex brain networks with parallel convolutional neural networks. The effectiveness of this model has been verified. In model visualization analysis, the visualization results of t-distribution random neighborhood embedding in the third separable convolutional layer indicate that the two types of imagination have already experienced separation. There is a clear boundary between the two at position 0 on both the horizontal and vertical axes. This is a significant improvement compared to the comparative model. In the model performance verification, the full band classification accuracy in the synchronous network was maintained between 60% to 84%, and the μ-rhythm was maintained between 59% to 81%. The average classification accuracy of the combined model was 77.40% with higher performance, which was higher than 68.53% and 70.87% of the single scale convolutional neural network. In comparison with deep learning algorithms, the average classification accuracy of the combined model was 85.74%, much higher than the 66.20% and 76.69% of the comparative models. The composite model constructed has good performance in recognizing and classifying electroencephalogram signals. It can be effectively applied in practical brain-computer interface technology or electroencephalogram signal analysis. The potential application area of this study in the future is the recognition and processing of complex EEG signals in medical institutions, which can improve the efficiency of signal processing in this field and reduce the manpower expenditure of medical personnel.

INDEX TERMS Frequency division multi feature complex brain network, parallel convolutional neural network, classification accuracy, full frequency band, synchronous network.

I. INTRODUCTION

The human brain is an extremely complex and mysterious system composed of many nerve cells. These neural cells interact with each other, forming a vast network closely related to human life activities such as thinking, cognition, language, and consciousness [1], [2]. Brain science is the most popular interdisciplinary field in the 21st century, which has inspired scientists to conduct detailed research on brain structure and function. Researchers hope to better understand and predict the complex working patterns of the human brain by studying the biological characteristics of different brain regions [3], [4]. Brain Computer Interface (BCI) is an emerging technology that has developed in recent years. It can achieve communication between the brain and the outside world by collecting electroencephalograms (EEG), avoiding traditional information input/output channels from transmitting information to the outside world (such as computers, machinery, etc.) [5]. The gradual development of BCI has led to its increasing application in evaluating, enhancing, assisting, replacing, and restoring the cognitive and sensory motor functions of people with disabilities. In addition, the continuous progress of bio-sensing technology has improved the recognition rate of EEG and promoted

The associate editor coordinating the review of this manuscript and approving it for publication was Feiqi Deng.

the rapid conversion of BCI [6]. However, BCI technology, which integrates multiple disciplines, is still in its early stages. Despite decades of research and fruitful results, there are still hidden dangers and challenges to overcome before achieving complete mind control. BCI technology is currently in the laboratory exploration stage. Meanwhile, the sampling frequency and accuracy of current EEG signal acquisition devices still cannot meet the requirements of BCI applicability. Therefore, this study combines frequency division multi feature complex brain network (FDMFCBN) with parallel convolutional neural network (PCNN) on the basis of fully analyzing the feature differences of complex brain networks in different rhythms. Based on this, the PCNN on Multi Band Brain Networks (MBBN-PCNN) is proposed. Its purpose is to improve the applicability of BCI, improve the efficiency and performance of EEG signal analysis, and provide theoretical support for the development of brain science and related disciplines.

The motivation for this research is that the current BCI technology has not yet achieved complete conceptual control, and the current EEG signal acquisition equipment lacks sampling frequency and accuracy, which limits the practicality of BCI technology. To improve the recognition and classification efficiency of EEG signals, researchers have proposed the MBBN-PCNN model. This model combines traditional neural networks with multi-feature complex brain networks after frequency division. The model was developed after in-depth analysis of the dynamic characteristics of complex brain networks. This model aims to enhance the accuracy of EEG signal analysis, mitigate the risks of BCIs in practical applications, and advance research in the field of neuroscience. Its goal is to provide a theoretical and technical foundation for the rehabilitation, medical research, and daily interaction of people with disabilities.

The paper is divided into four parts. The first part is a summary and discussion of the current research on complex networks or deep learning techniques in EEG signal analysis. The second part is to study the EEG signals of complex networks combined with convolutional neural networks (CNN), including the construction of FDMFCBN and the proposed MBBN-PCNN model. The third part is to verify the performance of the MBBN-PCNN model. The fourth part is a summary of the entire article.

II. RELATED WORK

Currently, there is an increasing amount of data in different fields, which requires an efficient method for data processing to extract and decode the rich information contained in the data. Machine learning, as a branch of artificial intelligence, does not require programming for specific tasks and has enormous learning efficiency. Deep learning, as a special subset of machine learning, has achieved advanced results in various fields such as object monitoring, speech recognition, and natural language processing [7]. In BCI systems, multi-channel EEG signals contain rich information that can be automatically analyzed for this specific type of data through deep learning, providing valuable output for the new generation of BCI systems [8]. Many scholars have conducted research on it. Li et al. proposed a model for driver attention dispersion detection based on deep learning to address the traffic safety issue of distracted driving during actual driving, effectively improving traffic safety by using EEG signals as output [9]. Altaheri et al. comprehensively discussed the application of deep learning technology in EEG motor imagery classification, aiming to address relevant issues in the practical application of BIC, providing direction for the development of BIC in healthcare [10]. Pandey and Seeja proposed a feature extraction technique for EEG signals by using variational pattern decomposition and deep learning to address the related issues of emotion recognition in EEG signals. This method effectively improved the performance of emotion recognition in EEG signals [11]. Afshar et al. proposed a combined deep learning architecture based on a detailed analysis of EEG in measuring anesthesia depth. This framework not only improved the accuracy of inter subject classification, but also improved the accuracy of anesthesia depth measurement [12].

In addition, Song and Xiao et al. proposed an evidence fusion method based on belief entropy visualization and complex networks to address the related issues in EEG signal fusion, effectively improving the accuracy of EEG signal dynamic fusion [13]. Khasawneh et al. proposed a new method for K-composite wave detection using deep transfer learning and complex networks to address the related issues in EEG signal detection. This method provided theoretical support for diagnosing neurophysiological disorders [14]. Dang et al. proposed a multi frequency multi-layer complex brain network using deep learning to address the related issues in EEG signal detection for epilepsy patients. This network effectively improved the accuracy of epilepsy EEG signal detection, and also provided a solution for EEG signals to represent the actual state of the brain [15]. Hussein et al. proposed a new method for driver drowsiness detection by analyzing EEG signals in detail and utilizing complex networks and deep learning to address the related issues in driver drowsiness detection. It provided data support for reducing driver damage caused by fatigue [16].

Akbari et al. found that early detection and treatment are crucial for preventing potential serious consequences in the diagnosis of depression. In recent years, researchers have begun to explore the use of graphic features of EEG signals to identify depression. This study adopted a set of newly extracted geometric features based on second-order differential graphs, and selected key features that are helpful for classification through binary particle swarm optimization (PSO) algorithm. Furthermore, applying these features to support vector machines (SVM) and K-nearest neighbor classifiers achieved an accuracy of up to 98.79%. The study found that the geometric features that were extracted and optimized were easier to recognize in images and improved classification accuracy by 17.56% compared to other features. This provides an efficient auxiliary tool

for early diagnosis of depression [17]. Akbari et al. also believed that the use of EEG signal processing technology is a highly promising research field in the diagnosis of epilepsy. Although analyzing EEG signals can be challenging due to their complexity and non-stationary nature, recent research has started to use Poincaré diagrams based on discrete wavelet transform coefficients to extract features from a geometric perspective. This approach can distinguish between epileptic and non-epileptic states. This article presents a new method for extracting geometric features. The method calculates standard descriptors, the sum of triangle areas, the sum of shortest distances relative to 45-degree lines, and the sum of distances of each point relative to the coordinate center. Binary PSO technology is used for feature selection. Using k-nearest neighbors and SVM classifiers to classify features, the research results showed that the proposed method could achieve a classification accuracy of up to 99.3%. This indicates the importance of the new geometric features derived from the Poincar é diagram in accurately identifying EEG signals, and provides a new perspective for the recognition of graphic features of EEG signals [18].

Studies by both domestic and foreign scholars have revealed that complete concept control of BIC still poses hidden dangers. Additionally, EEG signal acquisition devices suffer from issues with low sampling frequency and accuracy. At the same time, traditional EEG signal feature extraction algorithms do not consider the dependency relationships between brain regions during imaginative tasks. Therefore, the MBBN-PCNN model proposed in this study is innovative. It innovatively constructed a multi feature brain network by determining the optimal time window and introducing a frequency division strategy. Moreover, a time-domain data augmentation algorithm is used to expand the EEG signal data to avoid over-fitting issues that may arise from small datasets of EEG signals. Meanwhile, the MBBN-PCNN model itself improves the performance of complex brain networks decoded on the basis of EEG signals.

III. EEG SIGNALS OF COMPLEX NETWORKS COMBINED WITH CNN

The conventional method for analyzing EEG involves separating the positional signals of each lead to extract their features. However, the low spatial resolution of EEG signals significantly impacts their extraction effect. Sadiq et al. believe that CNN can effectively recognize fuzzy signals and improve recognition efficiency in EEG classification. Through automatic feature extraction, enhanced robustness, and efficient computation, it significantly optimizes the accuracy and speed of signal processing [19], [20]. Therefore, this section mainly analyzes the combination of FDMFCBN and PCNN.

A. CONSTRUCTION OF FDMFCBN

Currently, there are still hidden dangers in the complete control of ideas in BCI, and the sampling frequency and accuracy of EEG signal acquisition equipment are very low. Therefore, this study examines the interdependence of various brain regions in conscious tasks. It combines FDMFCBN with PCNN after analyzing the differences in the characteristics of complex brain networks at different rhythms, resulting in the proposal of MBBN-PCNN. Before constructing FDMFCBN, this study first analyzed EEG signal processing and classification. The EEG signals will be collected using a self-developed multi-channel perceptual Chinese character silent reading experiment. This will provide EEG information from multi-channel perceptual tasks and allow for exploration of the correlation between different brain regions in multimodal perceptual tasks. It proposes corresponding hypotheses based on the phenomenon of word for word silent reading that occurs when people read relevant data in daily life. Compared to simply reading, silently reading text can better improve actual reading efficiency. To verify the validity of this conjecture, it introduces a conscious task of additional language imagination. The data used in this study is the single mode experimental paradigm, and the flow of an experiment is Figure 1.

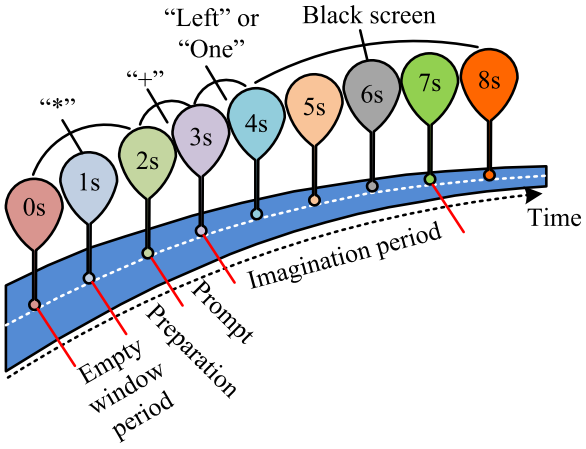

FIGURE 1. Flow diagram of an experiment under the single mode experiment paradigm.

In Figure 1, the experimental subjects follow the instructions on the screen and make corresponding thinking actions. After the experiment starts, there will be a "*" character in the center of the computer screen, and the subjects will have a waiting time of 2s. At this point, the screen will display the word "+", and the tester will have 1s to prepare. Then there is a 1s prompt, either "left" or "one" on the screen. The subjects imagine it for 4s on the screen. If it is "left", they kept imagining their body turning to the left. If it is "one", they imagine their handwritten "one". After 4s, the experiment ended and the subjects have a 1s rest time. Two prompts are randomly presented 15 times each. Throughout the entire experimental period, each participant is required to conduct 5 sets of experiments. After completing each group of experiments, the subjects are given a 5min rest period. In the end, 75 sets of experimental data are obtained for both types of imagination. In addition, in various conscious

activities, neurons in the brain produce various types of electrical waves. This study aims to systematically investigate the internal activities of the brain under different states of consciousness, using this wave as a starting point. The goal is to deepen the understanding of the complex working patterns and thinking processes of the human brain.

The computer-based BIC system converts the collected information into instructions, including both cranial electroencephalography, brain magnetic resonance imaging, and functional magnetic resonance imaging. In these studies, EEG signals can well reflect the physiological and pathological conditions of the human body, and have the advantages of simple acquisition, low cost, high time resolution, and easy portability. At the same time, using non-invasive methods to collect EEG from the outside of the scalp can reduce the risk of surgery and improve its convenience. Because EEG is a very small biological potential that is naturally generated by a large number of cells in the brain during conscious activities. Therefore, it requires extremely precise electronic devices for measurement. The EEG signal acquisition device used in this study is a SynAmps 2 sampler produced by Neuroscan Company, with a sampling frequency of 250 Hz. The device consists of electrodes, signal collectors, amplifiers, filters, and analog-to-digital converters. The experiment used a 35 channel electrode cap, which is consistent with the international EEG organization 10-20 system standard. The electrode cap is located in the primary motor area, Wernicke's area, Broca's area, and parietal lobule of the cortex. The impedance of each channel is below 5000 ohms, while the device uses a bandpass filter of 0.1-100 Hz.

Meanwhile, BIS systems utilizing Event Related Desynchronization/Event Related Synchronization (ERD/ERS) technology are currently a hot research topic. Among them, during motor imagination or actual exercise, there is an oscillation called ''sensory motor rhythm'' in the motor brain area. The reduction or increase of vibration is referred to as ''event dependent desynchronization'' and ''synchronization''. It is aimed at effectively extracting and quantifying the feature information contained in EEG signals. The concept of time-dependent spectral perturbation has been proposed, and its expression is equation (1).

$$E(b, e, \tau) = \frac{1}{m} \sum_{g=1}^{m} \left| Y_g(b, e, \tau, g) \right|^2 \tag{1}$$

In equation (1), E represents the disturbance value of the event correlation spectrum. b represents the channel. e represents frequency. τ represents time. g represents the number of data segments, with a maximum value of m. Y_g represents the time-frequency distribution value. The expression of ERD/ERS calculation is equation (2).

$$ERD/ERS = \frac{B - H}{H} \times 100\% \tag{2}$$

In equation (2), B represents the energy of the EEG signal in the same frequency band after the event occurred. H represents the relevant energy of the EEG filtered within a specific frequency band before the event (1s during the preparation period). The Common Space Pattern (CSP) is an efficient method for identifying ERD/ERS. By calculating two types of hypothetical covariance matrices, it greatly improves the intra class variance of the two types of hypothetical variances, thereby more efficiently extracting features of binary classification problems [21], [22]. However, CSP only recognizes spatial information with discriminative significance, while ignoring effective information in the frequency domain. Therefore, this study uses Filter Bank CSP (FBCSP) to perform corresponding spatial filtering on EEG signals. And by using mutual information selection method, two categories that may have significant differences are selected to ensure subsequent EEG signal analysis and classification recognition. At the same time, this study uses SVM to separate the optimal hyperplane from the training data of the second class imaginative EEG signal. Figure 2 shows the experimental process of FBCSP+SVM.

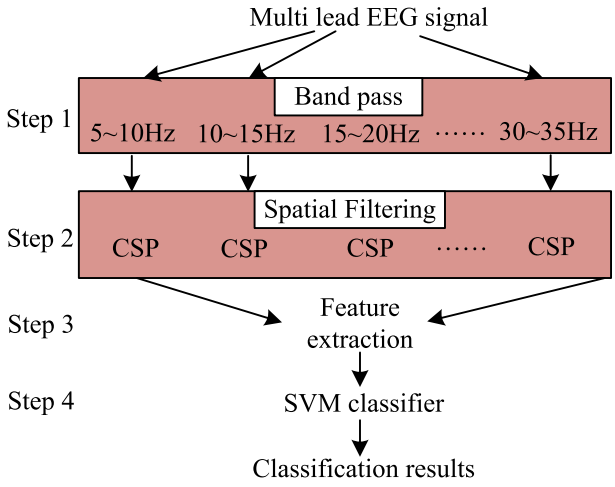

FIGURE 2. Schematic diagram of the experimental process of FBCSP+SVM.

In Figure 2, the experimental process of FBCSP+SVM first utilizes multiple sub-band filters to perform bandpass filtering on EEG signals, and then uses CSP spatial filtering to filter EEG signals in various frequency bands. On this basis, a feature selection method using mutual information is adopted to screen the features with maximum separability generated by multiple filter sets. Finally, SVM is used as the classifier, and the subject's 50 fold cross validation is used as the training classifier, with average accuracy as the evaluation indicator. Overall, it utilizes a parallel structure, with FBCSP consisting of multiple bandpass filters and spatial filters. The bandpass filter uses a zero phase Chebyshev II filter, and the spatial filter is used for CSP feature extraction. Based on the use of FBCSP+SVM for EEG classification, this study began to construct FDMFCBN. To build this network, it is necessary to synchronize the EEG signal, which includes correlation coefficients and phase locking values. The correlation coefficient analysis uses the cross-correlation function to construct actual complex brain

networks and measure the causal relationship between each pair of electrodes. It calculates the actual cross-correlation coefficient of EEG signals for each lead. Therefore, the expression of the cross-correlation coefficient between two temporal signals is equation (3).

$$G_{p,q}(t) = \frac{1}{N-t}\sum_{i=1}^{N-t}\left(\frac{p_i-\bar{p}}{\upsilon_p}\right)\left(\frac{q_i-\bar{q}}{\upsilon_q}\right) \quad (3)$$

In equation (3), $G_{p,q}$ represents the cross correlation function between the timing signals p and q. t represents the actual time delay between two types of signals. $\bar{p}$ and $\bar{q}$ represent the average values of two types of signals p and q. υ_p and υ_q represent the standard deviation of two types of signals. The value of the cross correlation coefficient is maintained between -1 and 1, where 1 represents the maximum positive correlation, 0 represents non correlation, and -1 represents the maximum negative correlation. The correlation coefficient exhibits symmetry, as expressed in equation (4).

$$G_{p,q}(t) = G_{q,p}(t) \quad (4)$$

In the analysis of phase locking values, phase synchronization does not rely on signal amplitude, but rather achieves mutual influence between EEG signals by observing the phase difference between them. In addition, the measurement of phase synchronization is also affected by certain frequency interference. Therefore, it is very important to process the information obtained from phase synchronization in various regions of the brain and establish information transmission in various brain regions. The expression of phase synchronization between EEG signals by leads is equation (5).

$$L_{p,q}(\tau) = \frac{1}{W}\left|\sum_{w=1}^{W}\exp\left(j\left\{\Delta\psi_w(\tau)\right\}\right)\right| \quad (5)$$

In equation (5), L represents the phase locking value. W represents the total number of samples in the time series. j represents an imaginary number. $\Delta\psi_w(\tau)$ represents the instantaneous phase difference related to the coordinate of the lead at time τ. The expression of instantaneous phase difference for the current channel of the W-th sample is equation (6).

$$\Delta\varnothing_w(\tau) = \left(\varnothing_p(\tau) - \varnothing_q(\tau)\right) \quad (6)$$

In equation (6), $\Delta\varnothing_w(\tau)$ represents the instantaneous phase difference. $\varnothing$ represents the phase value. The actual value range of phase locking value is maintained between 0 and 1. The larger the value, the more obvious the actual interaction between the two types of signals, and the stronger the phase synchronization, and vice versa. Therefore, based on the analysis of cross correlation function and phase locking value, the construction process of FDMFCBN is Figure 3.

In Figure 3, the construction process of FDMFCBN is first designed to eliminate signal redundancy by designing an optimal time window. Secondly, based on the spectral

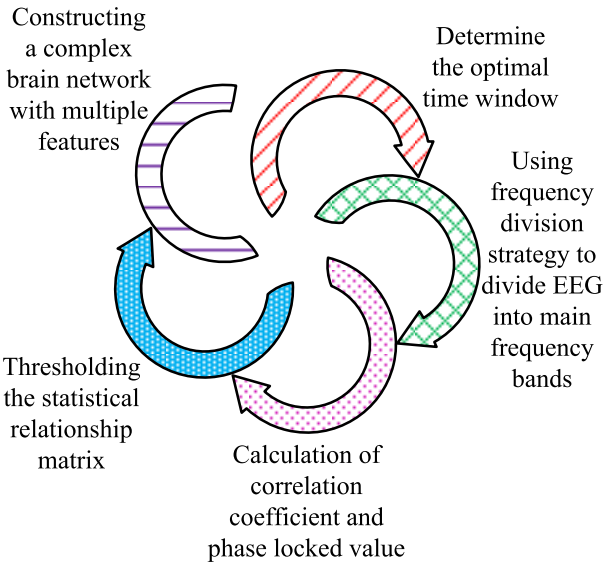

FIGURE 3. Schematic diagram of the construction process of FDMFCBN.

characteristics of the EEG signal, the main frequency band of the EEG signal is partitioned based on the frequency division strategy. Then, by calculating the correlation coefficients and phase locking values of each wire pair at different frequencies, a statistical relationship matrix of 35 * 35 is obtained for each scenario. Then, using the threshold method, two significantly different wire pairs are selected as feature information for fixed complex brain networks. Finally, a complex brain network with multiple features is established using leads as nodes and actual statistical relationships as node connection edges. To avoid the disruption of the connection structure of complex brain networks, this study conducts time-domain segmentation and reorganization of the experimental dataset, and proposes corresponding data augmentation methods. By utilizing the principle of time signal segmentation and recombination, the two types of imagined EEG signals are divided into three equal parts, and then the signal is recombined. Finally, a total of three measurements of the recombined signals are repeated to obtain a three fold synthesized time-domain enhanced EEG signal.

B. PCNN COMBINED WITH FDMFCBN

The dimensionality of FDMFCBN is relatively large, and blindly selecting traditional classifiers can easily lead to the loss of complex brain network structures when reducing the dimensionality of classifiers. Therefore, CNN was chosen as the training sample for the feature set, and MBBN-PCNN was proposed to classify EEG signals based on the time-frequency correlation of each lead. At present, deep learning has become a machine learning method suitable for large-scale and complex input data. Compared with traditional classification algorithms, neural networks have higher classification efficiency and stronger adaptability. But before inputting the data into the algorithm, it needs to be denoised using the Wavelet-

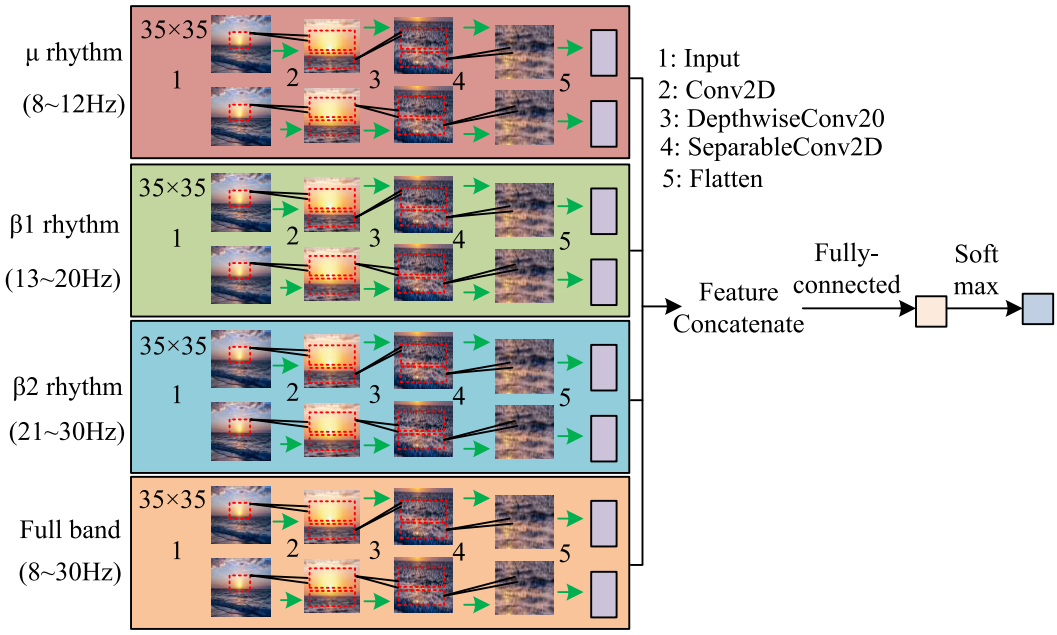

FIGURE 4. Schematic diagram of MBBN-PCNN network structure.

Based Principal Component Analysis (WBPCA) algorithm to minimize the impact of noise on the classification accuracy of EEG signals. The denoising algorithm WBPCA combines the statistical denoising ability of PCA with the time-frequency localization characteristics of wavelet transform, typically resulting in effective denoising outcomes. Sadiq et al. proposed three new intelligent task accurate classification frameworks and computer-aided diagnosis frameworks for the accurate recognition and classification of BCI images of EEG signals, respectively. Before the input of these two frameworks, the data set was first denoised by multi-scale principal components, and then empirical wavelet transform was carried out to divide the EEG signals into different modes. The author named MSPCA as the denoising method of mixed multi-scale principal component analysis and empirical wavelet transform. The test results show that the model recognition accuracy of MSPCA algorithm after noise removal is higher than the experimental results without noise processing [22], [23], [24]. Sadiq et al. also designed a denoising algorithm for EEG moving image decoding. The algorithm firstly uses multi-scale principal component analysis to improve the robustness of the recognition model against noise, and then uses multi-scale wavelet transform to process the data, which greatly reduces the complexity and computation of the recognition model. The author named this denoising model MEWT algorithm. The test results show that the EEG recognition model processed by MEWT algorithm has higher recognition accuracy and significantly faster calculation speed [25]. It can be seen that it is also necessary to use MSPCA algorithm to improve the quality of data sets before processing the model designed in this study.

EEG is a complex temporal spatial characteristic that is more difficult to interpret compared to text, images, files, etc. Therefore, this study aims to utilize deep learning technology to achieve automated processing of EEG data, providing valuable results for the next generation of BCI systems. Among them, the common structures of CNN include convolutional layer, pooling layer, and fully connected layer. The convolutional layer extracts features from the input data through convolutional verification, and its calculations are equations (7) and (8).

$$K_{output} = \frac{K_{input} - K_{filter} + 2\Im}{B} + 1 \tag{7}$$

In equation (7), K_{output} and K_{input} represent the width of the output and input data. $\Im$ represents the fill mode. B represents the convolutional kernel step size. K_{filter} represents the width of the filter data.

$$F_{output} = \frac{F_{input} - F_{filter} + 2\Im}{B} + 1 \tag{8}$$

In equation (8), F_{output} represents the high output data. F_{input} represents the high input data. F_{filter} represents the height of the filter data. When the actual filling mode is "same filling", regardless of the actual size of the convolutional kernel, the size of the input and output data is equal. Pooling layer is a feature manipulation method that passes through convolutional layers, which extracts kernel characteristics of input data by compressing it. Unlike convolutional layers, the operation sliding window of pooling layers does not have any parameters. At present, the mainstream sliding layer is divided into the maximum sliding layer and the average sliding layer, which are usually processed using sliding windows of different sizes. The maximum sliding layer is extracted from the sliding window, and the various feature quantities in the sliding window are accumulated and averaged to obtain the final result. The

function of the fully connected layer is to compress the features processed through convolution, pooling, etc., and ultimately achieve model classification. This method uses the weight parameters in the fully connected layer to compress the input features to the same number as the classification category. Then, it processes them through activation functions to improve the classification effect. The expression of the fully connected layer is equation (9).

$$T = \varpi \cdot \Re + \gamma \tag{9}$$

In equation (9), T represents the actual output vector. ϖ represents the weight vector. $\Re$ represents the implementation input vector. γ represents the offset. The fully connected layer is connected to the convolutional layer, and the output obtained from the convolutional layer is further used as the input of the fully connected layer. The main function of this layer is to process the feature maps extracted from the convolutional layer, and then serve as the next step for automatic classification, prediction, and other tasks. The output layers of commonly used CNN models include 1-2 fully connected layers. The fully connected layer is the classifier of CNN, forming an automatic classification task. In addition, the commonly used activation functions for CNN include S-type functions (Sigmaid), hyperbolic tangent functions (Tanh), rectified linear units (ReLu), and smooth linear rectification functions (Softplus). Sigmaid is the most commonly used activation function, which can also be understood as a normalization function due to its value range of [0, 1]. The derivative function of Sigmoid approaches zero infinitely, so it quickly reaches saturation state. The expression and derivative function of this function are shown in equation (10).

$$\begin{cases} y(x) = \dfrac{1}{1+e'^{-x}} \\ y'(x) = y(x)(1-y(x)) = \dfrac{e'^{-x}}{\left(1+e'^{-x}\right)^2} \end{cases} \tag{10}$$

In equation (10), $y(\cdot)$ represents the activation function. x represents the independent variable of the function. e' represents a natural constant. The Tanh function is widely used in nonlinear activation functions, with a range of $[-1, 1]$, thus possessing faster convergence performance. Tanh is expressed and derived as equation (11).

$$\begin{cases} y(x) = \dfrac{2}{1+e'^{-2x}} - 1 \\ y'(x) = 2y(x)\left[(1-y(x))\right] = \dfrac{4e'^{-2x}}{\left(1+e'^{-2x}\right)^2} \end{cases} \tag{11}$$

ReLu also belongs to the nonlinear activation function, which overcomes the problem of early saturation of Sigmoid. Its value range is $[0, +\infty)$, and the derivative function value range is $\{0,1\}$. The expressions of the two are shown in equation (12).

$$\begin{cases} y(x) = \max(0, x) \\ y'(x) = \begin{cases} 1, x > 0 \\ 0, x \le 0 \end{cases} \end{cases} \tag{12}$$

Finally, Softplus, as a logarithmic activation function, has a significant computational complexity. The value range of the Softplus function is $[0, +\infty)$. The expression and derivative function are shown in equation (13).

$$\begin{cases} y(x) = \log\left(1+e'^{x}\right) \\ y'(x) = \dfrac{e'^{x}}{1+e'^{x}} \end{cases} \tag{13}$$

Through the formulas of equations (10) to (13), the four commonly used activation functions are effective in dealing with simple CNN models, but there are difficulties in dealing with complex network problems. After comprehensive analysis, this study selected the traditional ReLu function, namely the Exponential Linear Unit (ELU), as shown in equation (14).

$$y(x) = \begin{cases} x, & x \ge 0 \\ \varphi\left(e'^{x} - 1\right), & x < 0 \end{cases} \tag{14}$$

In equation (14), φ represents the hyper-parameter that controls negative saturation. Compared with other activation functions such as ReLU and Tanh, the ELU function has been proven to improve the accuracy of training and testing. It is particularly useful in deep neural networks that require high accuracy. In addition, in practical applications, it is necessary to standardize the output vectors of the fully connected layer. This study selected the Softmax mapping function to standardize the data, as shown in equation (15).

$$z_\varsigma = softMax\left(\mu_\varsigma\right) = \frac{\exp\left(\mu_\varsigma\right)}{\sum_a \exp\left(\mu_a\right)} \tag{15}$$

In equation (15), z_ς represents the standardized result of the ς-th category. μ_ς represents the output value of the neural network for the ς-th category. a represents the output value of the total category. Softmax maps each output value of the CNN to a probability that the corresponding input sample pair identifies as a possible category. In recent years, a large number of studies have shown that CNN can efficiently extract effective features from EEG generated by motion imagination. At the same time, utilizing the multi structure deformation of CNN and integrating them with other structures can improve the classification ability of multi class EEG signals. Therefore, the actual MBBN-PCNN structure constructed in this study is Figure 4.

In Figure 4, the MBBN-PCNN structure is an end-to-end network for extracting and classifying EEG signals. Essentially, it is an improvement based on the EEG network. The network architecture adopts a parallel structure to extract features, selecting four different frequency bands (rhythm: μ, $\beta 1$, $\beta 2$, as well as full frequency band) multi feature brain

networks with parallel inputs from left to right to the CNN structure. To address individual differences in EEG signals, the feature matrices of the frequency division complex brain network are combined by the fully connected layer after passing through their respective convolutional layers. The resulting output is then sent to the Softmax classifier for classification. Each sub CNN in the parallel structure is composed of convolutional layers, deep convolutional layers, separable convolutional layers, average pooling layers, and fully connected layers. The first layer of convolution adopts four 1 * 6 convolution cores and achieves constant output size through ''Same padding''. Therefore, the result obtained by the first layer convolution is still 35 * 35. On this basis, a 35 * 1 deep convolution method is used to reduce the number of parameters in the fitting process. In addition, this study has also done a lot of normalization on the dimensionality of feature maps. To effectively improve the stability and robustness of the model, while taking into account the differences between different subject categories, a Dropout of 0.25 is selected.

Next, a 1 * 4 sliding window average pooling layer is used to compress input features and extract their core features. Then there is a separable convolution, consisting of point wise convolutions of 1 * 4 and 1 * 1. The features processed through the above construction are then processed using uniform pooling layers and flat layers, respectively. Finally, the fully connected layer is used to fuse the features of each sub network, achieving the optimal fusion of each sub network. These features are solved using the softmax function to obtain the probability of each type of EEG signal on each input variable. By introducing methods such as loss function and optimal function, the difference between the predicted results of the model and the actual data is measured to evaluate the generalization performance of the constructed model. This study uses class crossover approximation as the loss function and optimizes the model parameters using Stochastic Gradient Descent (SGD). Simultaneously, the ReduceLROnPlateau function in Bayesian networks is used to monitor the prediction results, adjust the learning rate, and improve the model's adaptive ability. The coefficient for each decrease in learning rate is set to 0.3, the lower limit of learning rate is set to 5e-5, and the batch size is 16.

IV. PERFORMANCE VERIFICATION OF MBBN-PCNN BASED ON FREQUENCY DIVISION FEATURE NETWORK AND CNN

Conducting experiments on a model is an important way to verify its effectiveness. Regarding EEG signals, verifying the performance of the model requires both accurate analysis and visual inspection. Therefore, this section mainly focuses on two aspects: the visual analysis and performance verification of the MBBN-PCNN model. Sadiq et al. proposed a new automation framework, which can carry out training of brain-computer interface system under the condition of small data samples, and the number of samples used in this research test is not less than 1000 conditions [23]. Yu et al. proposed a new automated computing framework in which the test Fourier decomposition is used to recognize motion and mental image EEG signals. Then, the author used MeI dataset with large sample size to conduct validation experiments on the design framework, and proved the robustness and computational efficiency of the design model [24]. The above previous research results show that the data set used in the design model performance verification experiment of this study is not easy to be too small.

A. VISUALIZATION ANALYSIS AND MODEL COMPARISON OF MBBN-PCNN MODEL

To verify the effectiveness of the constructed MBBN-PCNN structure in EEG signal analysis, this study first utilized t-Distributed Stochastic Neighbor Embedding (t-SNE) to reduce dimensionality and visualize the training situation of each layer in the neural network. The purpose is to observe more clearly the learning effectiveness of the brain network at various layers and the differences between different models. Before this, the first is to set the substructure parameters of MBBN-PCNN, as shown in Table 1.

In Table 1, the number, size, and output size of convolutional kernels in the substructure of MBBN-PCNN are 4, 1×16, and $35 \times 35 \times 4$, respectively. The deep convolutional layers are 8, 35×1, and $1 \times 35 \times 8$, respectively. The separable convolutional layers are 8, 1×4, and $1 \times 8 \times 8$, respectively. Based on the setting of substructure parameters, 5000 subjects were selected for the experiment, including 2466 males and 2534 females, aged from 22 to 28 years old, with good health status and visual correction. For the convenience of statistics, these subjects were randomly and evenly divided into 10 groups, and each group was set as H1∼H10 groups, and all subjects signed the ''Informed Consent Form''. Before the experiment begins, it is necessary to ensure that the subjects have sufficient rest time and prohibit drinking coffee, tea, and alcoholic beverages. Among them, members of the H1-H7 groups underwent language imagination experiments, but did not participate in body rotation and writing stroke imagination experiments. In this experiment, both of their hands naturally relaxed. Therefore, group H9 is subjected as an example, the t-SNE visualization results of the first and second deep convolutional layers of the MBBN-PCNN model are shown in Figure 5.

According to Figure 5, the t-SNE visualization results of the first convolutional layer indicate that there is no significant difference between the two types of imagination. There are many overlapping areas, and most of them overlap when the values are between 0 and 10. The visualization results of the second deep convolutional layer t-SNE show that there is still a significant overlap between the two types of imagination, with values mainly distributed between 0 and 10. The visualization results of t-SNE for the third separable convolutional layer and the fourth fully connected layer are shown in Figure 6.

Based on Figure 6, in the visualization results of the third separable convolutional layer t-SNE, there is already a sep-

TABLE 1. Result of substructure parameter setting for MBBN-PCNN.

layer type	Number of convolutional kernels	Size	Output Size	Mode
Input	-		35×35×1	-
Convolutional Layer	4	1×16	35×35×4	Same padding
Deep convolutional layer	8	35×1	1×35×8	Valid padding
Average pooling layer	-	1×4	1×8×8	-
Separable convolutional layer	8	1×4	1×8×8	Same padding
Average pooling layer		1×4	1×2×8	
Flat layer	-	-	16	-
Fully connected layer			2	

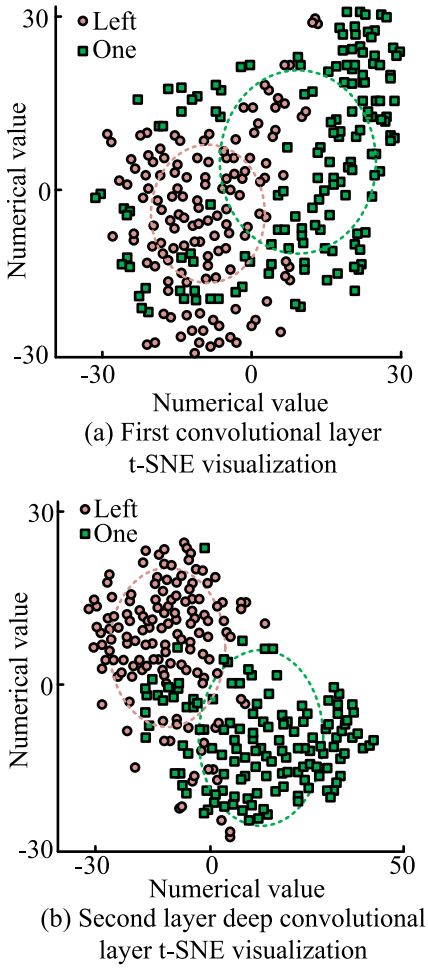

FIGURE 5. t-SNE visualization results of the first and second deep convolutional layers in the MBBN-PCNN model.

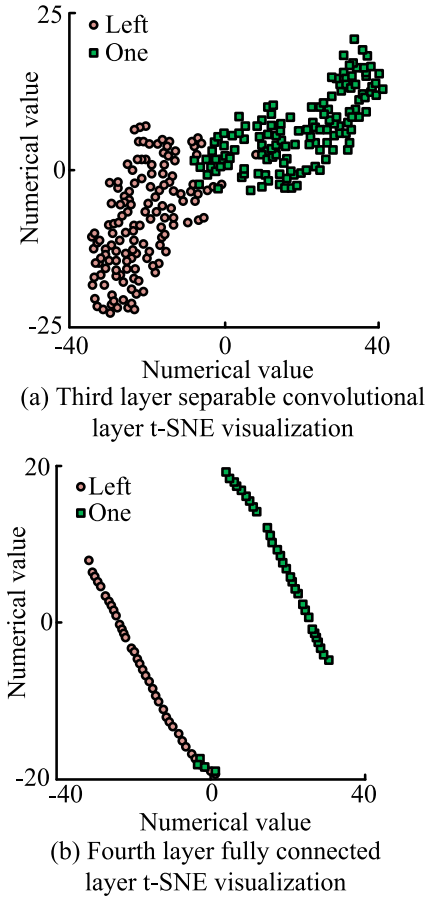

FIGURE 6. Visualization results of t-SNE for the third separable convolutional layer and the fourth fully connected layer.

aration phenomenon between the two types of imagination, with a clear boundary between them near the horizontal and vertical axis of 0. In the visualization results of the fourth fully connected layer t-SNE, the two types of imagination have shown good distinguishability. Figures 5 and 6 indicate that the proposed MBBN-PCNN model has high recognition and classification performance, and can effectively analyze and distinguish between two types of signals. To further verify the superiority of MBBN-PCNN, this study introduces Shallow Convolutional Network (Shallow ConvNet) and Deep Convolutional Network (DeepConvNet) for comparison. The Shallow ConvNet, a CNN architecture, is frequently utilized for classifying oscillatory signals. However, its performance in classifying EEG signals related to event-related potentials is not exceptional. Meanwhile, Deep ConvNet is not limited to specific input types due to its deep architecture. Therefore, to verify the effectiveness of MBBN-PCNN, this study improved both and designed parallel structured Shallow ConvNet and Deep ConvNet models. The sub route structural parameters of the improved two models are shown in Table 2.

In Table 2, 0-9 represent the input first convolutional layer, second convolutional layer, average pooling layer, flat layer, fully connected layer, maximum pooling layer, third convolutional layer, fourth convolutional layer, and fifth convolutional layer, respectively. The improved Shallow ConvNet has 10 and 5 two-layer convolutional kernels in its sub route structure parameters, with sizes of 1 × 16 and

TABLE 2. The sub route structural parameters of the improved two comparative models.

Improved ShallowConvNet's sub route structural parameters			
layer type	Number of convolutional kernels	Size	Output Size
0	-		35×35×1
1	10	1×16	35×20×10
2	5	8×16	28×5×5
3		1×2	28×2×5
4	-		280
5		-	2
Improved Subroute Structure Parameters for DeepConvNet			
layer type	Number of convolutional kernels	Size	Output Size
0	-		35×35×1
1	10	1×2	35×34×10
2	10	35×1	1×34×10
6	-	1×2	1×17×10
7	10	1×2	1×16×10
6	-	1×2	1×8×10
8	10	1×2	1×7×10
6	-	1×2	1×3×10
9	10	1×2	1×2×10
6		1×4	1×1×10
4	-		10
5		-	2

8 × 16, respectively. The improved Deep ConvNet has 10 convolutional kernels per layer in the sub route structure parameters, and the output size decreases as the convolutional layers increase. Under this parameter, group H9 is subjected as an example, the t-SNE visualization results of the first and fully connected layers of Shallow ConvNet are shown in Figure 7.

In Figure 7, there is a significant overlap between the two types of imagination in the first convolutional layer of the Shallow ConvNet model, and the distribution remains basically consistent. The results of the fully connected layer show that there is a clear overlap between the two types of imagination, and there is no significant boundary. Comparing Figures 5 and 6, the classification performance of the Shallow ConvNet model is much lower than that of the MBBN-PCNN model. The t-SNE visualization results of the first and fully connected layers of Deep ConvNet are shown in Figure 8.

In Figure 8, there is also a significant overlap between the two types of imagination in the first convolutional layer of the Deep ConvNet model, but there is already a certain degree of differentiation compared to the Shallow ConvNet model. From a structural perspective, there are clear boundaries in the Deep ConvNet model, and the classification effect has already met the requirements. Compared to Figures 5-8, the MBBN-PCNN model demonstrates a more significant effect in actual feature learning in each layer, particularly in the fully connected layer. The research model has a stronger ability to distinguish between the two types of EEG signals. This result indicates that the proposed PCNN using FDMFCBN has high feasibility and rationality.

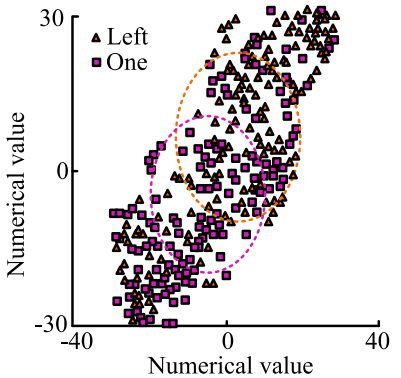

(a) ShallowConvNet First Convolutional Layer t-SNE Visualization

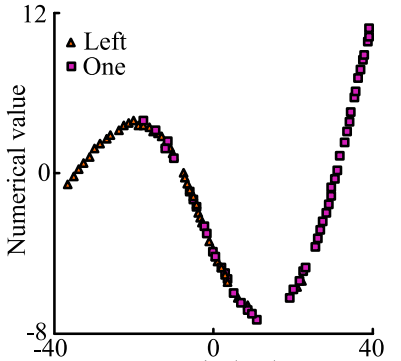

(b) ShallowConvNet fully connected layer t-SNE visualization

FIGURE 7. t-SNE visualization results of ShallowConvNet's first and fully connected layers.

B. ACCURACY AND STABILITY ANALYSIS OF MBBN-PCNN

To further verify the accuracy and stability of MBBN-PCNN, this study used a self collected EEG dataset. The dataset is still generated by 5000 participants, each of whom underwent 75 experiments of imagining handwritten "one" character and 75 experiments of imagining left hand rotation of the body. The experiment used a 10 fold cross validation

TABLE 3. Comparison of improved ShallowConvNet and DeepConvNet with research models.

Subject	Improved ShallowConvNet	Improved DeepConvNet	MBBN-PCNN
H1	77.31±8.82%	91.98±5.83%	95.54±3.61%
H2	68.20±7.01%	57.98±7.64%	79.78±9.11%
H3	72.87±7.15%	83.76±6.18%	89.31±8.86%
H4	61.09±3.93%	78.87±9.13%	86.20±7.52%
H5	49.98±1.15%	66.65±7.31%	72.20±11.08%
H6	79.31±7.89%	77.76±8.87%	89.54±6.09%
H7	59.54±8.35%	73.31±11.50%	78.20±6.07%
H8	49.98±1.15%	67.09±6.25%	79.31±6.85%
H9	79.76±10.63%	93.76±6.25%	96.87±2.83%
H10	63.98±5.89%	75.76±10.11%	90.20±5.03%
Average	66.20%	76.69%	85.74%

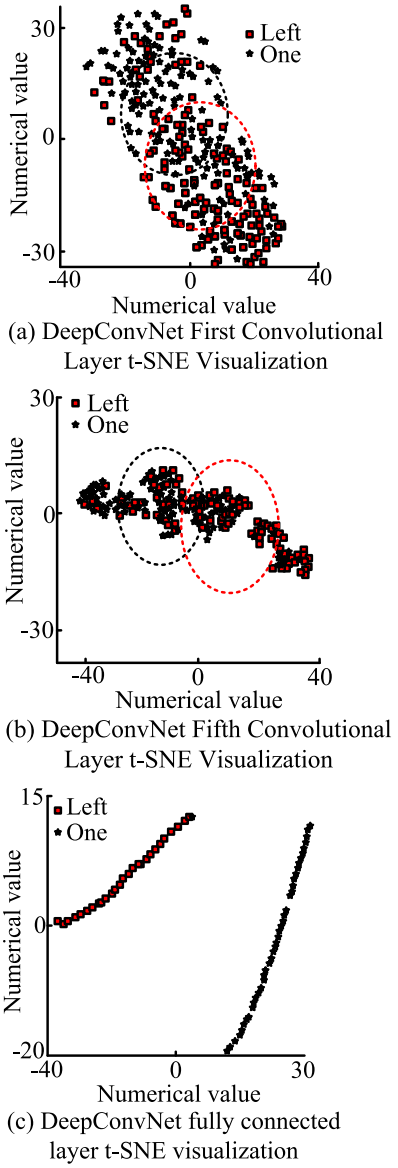

FIGURE 8. t-SNE visualization results of DeepConvNet's first and fully connected layers.

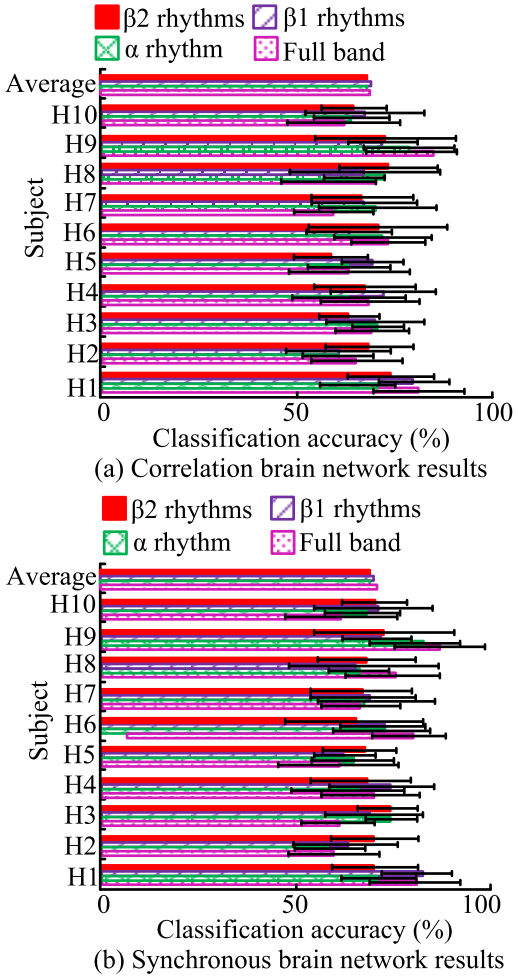

FIGURE 9. Classification accuracy results of single size CNN input for correlation networks and synchronization networks in various frequency bands.

method, dividing various EEG signal datasets into ten groups, named H1∼H10. Each time, one group was selected as the test set, and the remaining set was used as the training set. The experiment was repeated ten times. To calculate the average accuracy of the last 10 classification results and the standard deviation of the 10 classification results. Firstly, the frequency division multi feature brain network is input into a single size CNN, and the classification accuracy results of each frequency band correlation network and synchronization network input into a single size CNN are shown in Figure 9.

In Figure 9, the full band classification accuracy in the correlation network is maintained between 58% to 85%, rhythm μ is maintained between 60% to 78%, $\beta 1$ is maintained between 61% to 80%, and $\beta 2$ is maintained between 58% to 75%. In synchronous networks, the accuracy of full band classification is maintained between 60% to 84%, with rhythms μ ranging from 59% to 81%, $\beta 1$ ranging from 62% to 82%, and $\beta 2$ ranging from 63% to 73%. Overall, compared to relevant brain area networks, neural networks characterized by synchronous brain networks have better classification performance. The complex brain networks with rhythms μ and $\beta 1$ have higher classification accuracy, indicating that these two bands have stronger correlation in two types of consciousness tasks. On the basis of this result, the classification results of the full frequency band correlated brain network and synchronized brain network input single size CNN and frequency division multi feature brain network models are compared as shown in Figure 10.

From Figure 10, the MBBN-PCNN model has classification accuracy of 98.72 ± 0.41%, 98.40 ± 0.39%, 99.21 ± 0.57%, 99.14 ± 0.68%, 98.65 ± 0.63%, 99.02 ± 0.74%, and 98.52 ± 0.49% in the subject groups H1-H5, H7, and H10, respectively, which are higher than the single size CNN model. However, the EEG resolution accuracy of the Multivariational modal decomposition algorithm (Multivariate Variational Mode Decomposition, MVMD) method designed in the study of literature [23] was 93% in the subject independent experiment, and the EEG resolution accuracy of the Maximum empirical wavelet transform algorithm (Maximal Empirical Wavelet Transform, MEWT) method designed in the study of literature [24] was 88.08%∼92.82% in multiple data sets, indicating that the design method of this study also had certain performance advantages compared with the two literature.

The MBBN-PCNN model has higher classification accuracy and significantly improves performance compared to single size structures. To verify the reliability of the data augmentation method used in this study, a multi feature complex brain network established by artificially synthesized data in various frequency bands was inputted into a single size CNN for classification accuracy comparison. Figure 11 shows the results.

In Figure 11, the complex brain network established by strengthening the data can effectively improve the recognition accuracy of the model while increasing the sample size. Two types of μ-rhythm show higher classification accuracy in different brain regions. Synchronous brain networks in each band, as single dimensional inputs, have higher classification accuracy than related brain networks. Therefore, it is more effective to study the interaction between brain regions by observing the phase difference between signals. Figure 12 shows the comparison results with the MBBN-PCNN model.

In Figure 12, the classification accuracy of the MBBN-PCNN model among 5000 subjects was higher than that of the comparison model, with the highest classification accuracy reaching 96.89 ± 2.85%. Among various training

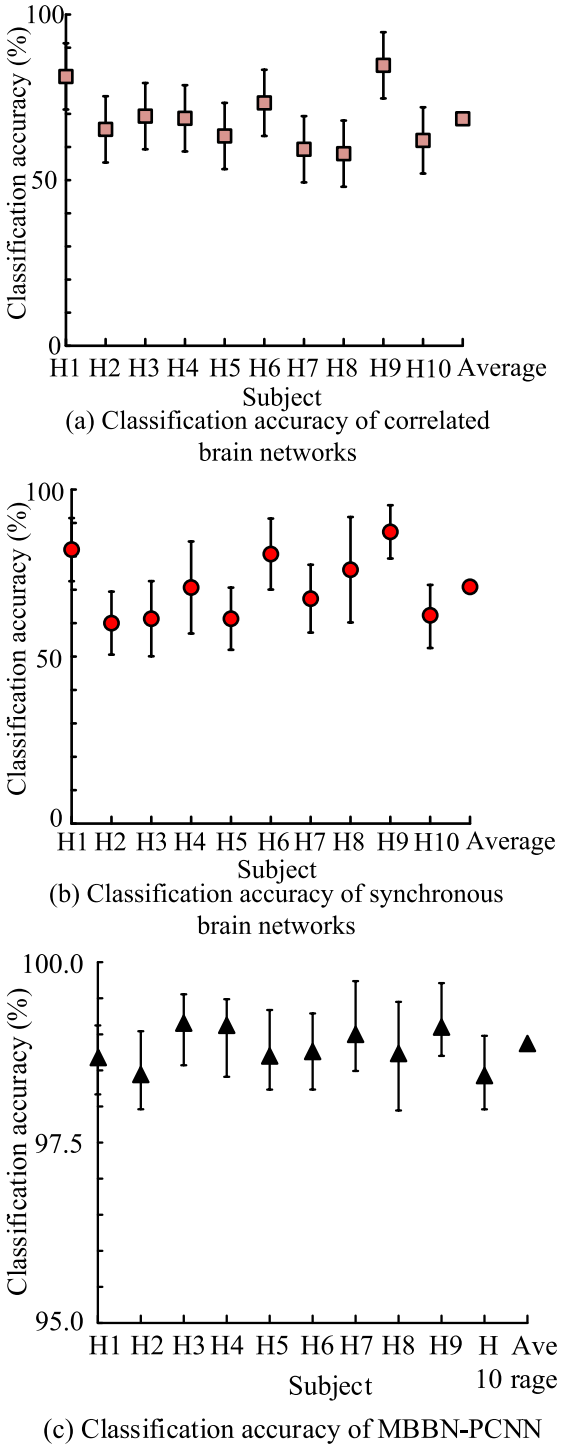

FIGURE 10. Comparison between single size CNN and MBBN-PCNN.

methods, multi-scale CNN has good learning performance. Compared with the pre training method using frequency division multi feature network training, this method can improve the classification accuracy of training samples by 8.36%. Meanwhile, the classification performance of PCNN is significantly higher than that of single size models, once again proving that the research model has significantly

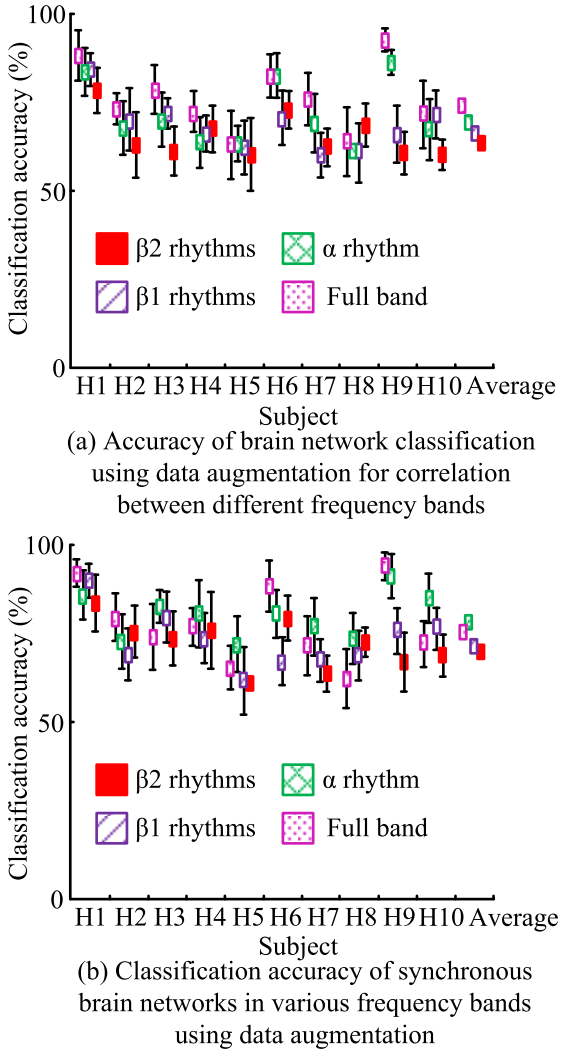

FIGURE 11. Comparison of correlation and synchronization network classification accuracy of EEG signals after data enhancement in various frequency bands.

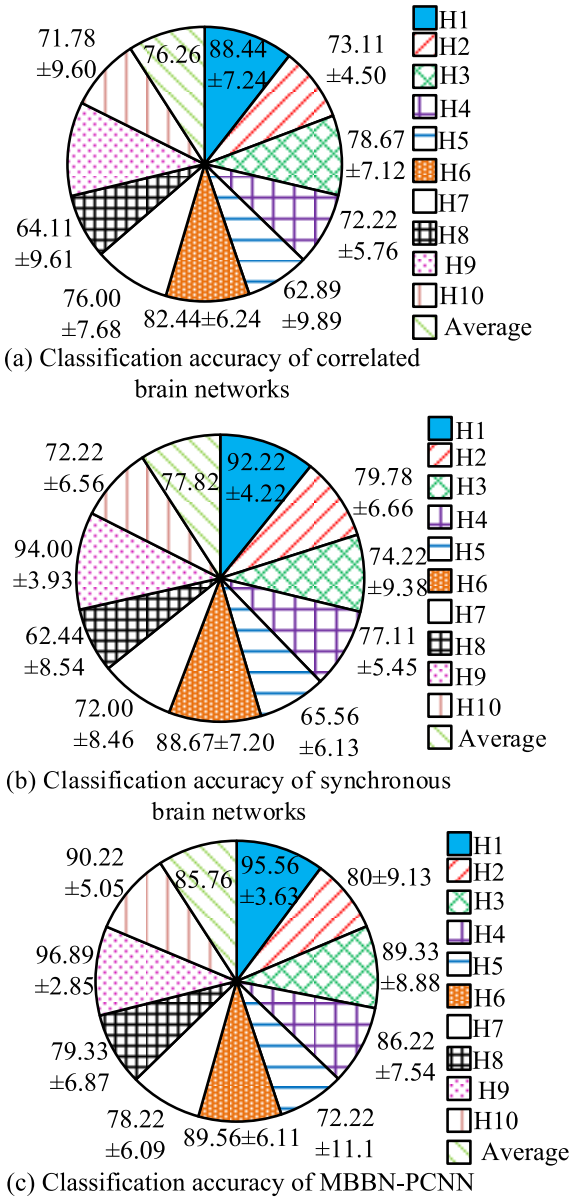

FIGURE 12. Comparison of single scale CNN data enhancement results with MBBN-PCNN model results.

improved performance compared to single size structures. Finally, this study also compared it with the improved Shallow ConvNet model and Deep ConvNet model, and the results are shown in Table 3.

In Table 3, the average classification accuracy of MBBN-PCNN reaches 85.74%, much higher than the 66.20% and 76.69% of the comparative models. Overall, the MBBN-PCNN model is more feasible and reasonable compared to both shallow and deep CNN structures with the best classification performance, high accuracy, and stable performance.

To fully compare the performance of the designed EEG signal recognition models, advanced EEG Network (EEG-Net), Temporal Spatial Recurrent Neural Network (TSRNN), and Graph Signal Processing Network (GSPN) were selected to compare the models for recognition experiments. The results are summarized in Table 4. Based on Table 4, the MBBN-PCNN model designed in this study demonstrates higher recognition accuracy than the other compared models, both in terms of the mean values of each group and all group data.

V. RESEARCH CONTRIBUTION

The research team's pioneering combination of FDMFCBNs and PCNNs resulted in the MBBN-PCNN model, which contributes to the existing knowledge system. This model shows excellent performance in EEG signal analysis, particularly in terms of classification accuracy when compared to single scale CNN and traditional methods. This study provides an effective tool for achieving high-precision EEG signal recognition and promotes the development of BCI technology. It has guiding significance for the cross-fusion of brain science and computational neuroscience.

TABLE 4. Comparison of accuracy between Mbbn-Pcnn and various advanced eeg signal recognition models.

Data set	MBBN-PCNN	EEGNet	TSRNN	GSPN
H1	99.5%	96.5%	94.6%	92.7%
H2	99.3%	96.3%	95.5%	93.1%
H3	99.5%	96.4%	94.8%	91.9%
H4	99.4%	96.6%	93.6%	92.6%
H5	99.4%	97.0%	95.2%	93.8%
H6	99.4%	96.9%	94.5%	92.5%
H7	99.4%	96.2%	93.3%	91.3%
H8	99.5%	97.1%	95.0%	93.0%
H9	99.6%	96.8%	94.7%	92.8%
H10	99.6%	97.3%	94.9%	94.0%
Average	99.4%	96.7%	94.6%	92.9%

VI. CONCLUSION

The MBBN-PCNN model was proposed in this study and its effectiveness in addressing the current hidden dangers of complete ideation control in BCI and the low sampling frequency and accuracy of EEG signal acquisition equipment was verified. The experimental data showed that in the visualization results of the third separable convolutional layer t-SNE, there was already a separation phenomenon between the two types of imagination, with a clear boundary between the two near position 0 on the horizontal and vertical axes. This study proposed the MBBN-PCNN model, which effectively addresses the hidden dangers of complete ideation control in BCI and the low sampling frequency and accuracy of EEG signal acquisition equipment. Compared with relevant brain area networks, neural networks characterized by synchronous brain networks had better classification performance. The MBBN-PCNN model achieved high classification accuracy in subject groups H1-H5, H7, and H10, with values ranging from 98.40% to 99.21%. These values were higher than those obtained by the single size CNN model. At the same time, the complex brain network established by strengthening the data could effectively improve the recognition accuracy of the model while increasing the sample size. And the average classification accuracy of MBBN-PCNN reached 85.74%, which was also better than the comparison model. Overall, the proposed MBBN-PCNN models were more feasible and reasonable. However, the experiments conducted in this study were all based on the self-developed dataset. In the future, the proposed model needs to be applied to a common dataset for more accurate analysis of EEG signals. For the MBBN-PCNN model proposed in this study, future research should focus on applying the model to a wider and more diverse public dataset to verify its ability to generalize and identify different types of EEG signals. Further work can explore the real-time application capabilities of the model, such as real-time EEG monitoring and real-time feedback systems. Furthermore, due to the significant variability in human brain activity, future research should prioritize enhancing model adaptability to individual differences and integrating multiple brain science theories to optimize network structures. This will enable more precise analysis of EEG signals.

REFERENCES

[1] Y. Mohammadi and M. H. Moradi, "Prediction of depression severity scores based on functional connectivity and complexity of the EEG signal," *Clin. EEG Neurosci.*, vol. 52, no. 1, pp. 52–60, Jan. 2021, doi: 10.1177/1550059420965431.

[2] P. M. Rossini, F. Miraglia, and F. Vecchio, "Early dementia diagnosis, MCI-to-dementia risk prediction, and the role of machine learning methods for feature extraction from integrated biomarkers, in particular for EEG signal analysis," *Alzheimer's Dementia*, vol. 18, no. 12, pp. 2699–2706, Apr. 2022, doi: 10.1002/alz.12645.

[3] Z. Aslan and M. Akin, "A deep learning approach in automated detection of schizophrenia using Scalogram images of EEG signals," *Phys. Eng. Sci. Med.*, vol. 45, no. 1, pp. 83–96, Mar. 2022, doi: 10.1007/s13246-021-01083-2.

[4] D. Merlin Praveena, D. Angelin Sarah, and S. Thomas George, "Deep learning techniques for EEG signal applications—A review," *IETE J. Res.*, vol. 68, no. 4, pp. 3030–3037, Jul. 2022, doi: 10.1080/03772063.2020.1749143.

[5] S. K. Khare, V. Bajaj, and U. R. Acharya, "PDCNNet: An automatic framework for the detection of Parkinson's disease using EEG signals," *IEEE Sensors J.*, vol. 21, no. 15, pp. 17017–17024, Aug. 2021, doi: 10.1109/JSEN.2021.3080135.

[6] X. Zhong, Y. Gu, Y. Luo, X. Zeng, and G. Liu, "Bi-hemisphere asymmetric attention network: Recognizing emotion from EEG signals based on the transformer," *Appl. Intell.*, vol. 53, no. 12, pp. 15278–15294, Nov. 2023, doi: 10.1007/s10489-022-04228-2.

[7] Y. Yang and X. Song, "Research on face intelligent perception technology integrating deep learning under different illumination intensities," *J. Comput. Cognit. Eng.*, vol. 1, no. 1, pp. 32–36, Jan. 2022, doi: 10.47852/bonviewjcce19919.

[8] Q. Kang, Q. Gao, Y. Song, Z. Tian, Y. Yang, Z. Mao, and E. Dong, "Emotion recognition from EEG signals of hearing-impaired people using stacking ensemble learning framework based on a novel brain network," *IEEE Sensors J.*, vol. 21, no. 20, pp. 23245–23255, Oct. 2021, doi: 10.1109/JSEN.2021.3108471.

[9] G. Li, W. Yan, S. Li, X. Qu, W. Chu, and D. Cao, "A temporal–spatial deep learning approach for driver distraction detection based on EEG signals," *IEEE Trans. Autom. Sci. Eng.*, vol. 19, no. 4, pp. 2665–2677, Oct. 2022, doi: 10.1109/TASE.2021.3088897.

[10] H. Altaheri, G. Muhammad, M. Alsulaiman, S. U. Amin, G. A. Altuwaijri, W. Abdul, M. A. Bencherif, and M. Faisal, "Deep learning techniques for classification of electroencephalogram (EEG) motor imagery (MI) signals: A review," *Neural Comput. Appl.*, vol. 35, no. 20, pp. 14681–14722, Jul. 2023, doi: 10.1007/s00521-021-06352-5.

[11] P. Pandey and K. R. Seeja, "Subject independent emotion recognition from EEG using VMD and deep learning," *J. King Saud Univ. Comput. Inf. Sci.*, vol. 34, no. 5, pp. 1730–1738, May 2022, doi: 10.1016/j.jksuci.2019.11.003.

[12] S. Afshar, R. Boostani, and S. Sanei, "A combinatorial deep learning structure for precise depth of anesthesia estimation from EEG signals," *IEEE J. Biomed. Health Informat.*, vol. 25, no. 9, pp. 3408–3415, Sep. 2021, doi: 10.1109/JBHI.2021.3068481.

[13] X. Song and F. Xiao, "Combining time-series evidence: A complex network model based on a visibility graph and belief entropy," *Appl. Intell.*, vol. 52, no. 9, pp. 10706–10715, Jan. 2022, doi: 10.1007/s10489-021-02956-5.

[14] N. Khasawneh, M. Fraiwan, and L. Fraiwan, "Detection of K-complexes in EEG signals using deep transfer learning and YOLOv3," *Cluster Comput.*, vol. 26, no. 6, pp. 3985–3995, Dec. 2023, doi: 10.1007/s10586-022-03802-0.

[15] W. Dang, D. Lv, L. Rui, Z. Liu, G. Chen, and Z. Gao, "Studying multi-frequency multilayer brain network via deep learning for EEG-based epilepsy detection," *IEEE Sensors J.*, vol. 21, no. 24, pp. 27651–27658, Dec. 2021, doi: 10.1109/JSEN.2021.3119411.

[16] R. M. Hussein, F. S. Miften, and L. E. George, "Driver drowsiness detection methods using EEG signals: A systematic review," *Comput. Methods Biomechanics Biomed. Eng.*, vol. 26, no. 11, pp. 1237–1249, Aug. 2023, doi: 10.1080/10255842.2022.2112574.
[17] H. Akbari, M. T. Sadiq, M. Payan, S. S. Esmaili, H. Baghri, and H. Bagheri, "Depression detection based on geometrical features extracted from SODP shape of EEG signals and binary PSO," *Traitement du Signal*, vol. 38, no. 1, pp. 13–26, Feb. 2021, doi: 10.18280/ts.380102.
[18] H. Akbari, M. T. Sadiq, N. Jafari, J. Too, N. Mikaeilvand, A. Cicone, and S. Serra-Capizzano, "Recognizing seizure using Poincaré plot of EEG signals and graphical features in DWT domain," *Bratislava Med. J.*, vol. 124, no. 1, pp. 12–24, Jan. 2022, doi: 10.4149/bll_2023_002.
[19] C. L. Grady, J. R. Rieck, D. Nichol, K. M. Rodrigue, and K. M. Kennedy, "Influence of sample size and analytic approach on stability and interpretation of brain-behavior correlations in task-related fMRI data," *Hum. Brain Mapping*, vol. 42, no. 1, pp. 204–219, Sep. 2020, doi: 10.1002/hbm.25217.
[20] J. Sorinas, J. C. F. Troyano, J. M. Ferrández, and E. Fernandez, "Unraveling the development of an algorithm for recognizing primary emotions through electroencephalography," *Int. J. Neural Syst.*, vol. 33, no. 1, Jan. 2023, Art. no. 2250057, doi: 10.1142/s0129065722500575.
[21] W. Li, B. Hou, X. Li, Z. Qiu, B. Peng, and Y. Tian, "TMLP+SRDANN: A domain adaptation method for EEG-based emotion recognition," *Measurement*, vol. 207, Feb. 2023, Art. no. 112379, doi: 10.1016/j.measurement.2022.112379.
[22] M. T. Sadiq, X. Yu, Z. Yuan, and M. Z. Aziz, "Motor imagery BCI classification based on novel two-dimensional modelling in empirical wavelet transform," *Electron. Lett.*, vol. 56, no. 25, pp. 1367–1369, Oct. 2020, doi: 10.1049/el.2020.2509.
[23] M. T. Sadiq, X. Yu, Z. Yuan, M. Z. Aziz, N. U. Rehman, W. Ding, and G. Xiao, "Motor imagery BCI classification based on multivariate variational mode decomposition," *IEEE Trans. Emerg. Topics Comput. Intell.*, vol. 6, no. 5, pp. 1177–1189, Oct. 2022, doi: 10.1109/TETCI.2022.3147030.
[24] M. T. Sadiq, X. Yu, Z. Yuan, F. Zeming, A. U. Rehman, I. Ullah, G. Li, and G. Xiao, "Motor imagery EEG signals decoding by multivariate empirical wavelet transform-based framework for robust brain–computer interfaces," *IEEE Access*, vol. 7, pp. 171431–171451, 2019, doi: 10.1109/ACCESS.2019.2956018.
[25] M. T. Sadiq, H. Akbari, S. Siuly, Y. Li, and P. Wen, "Alcoholic EEG signals recognition based on phase space dynamic and geometrical features," *Chaos, Solitons Fractals*, vol. 158, May 2022, Art. no. 112036, doi: 10.1016/j.chaos.2022.112036.
[26] M. T. Sadiq, X. Yu, Z. Yuan, M. Z. Aziz, S. Siuly, and W. Ding, "Toward the development of versatile brain–computer interfaces," *IEEE Trans. Artif. Intell.*, vol. 2, no. 4, pp. 314–328, Aug. 2021, doi: 10.1109/TAI.2021.3097307.
[27] X. Yu, M. Z. Aziz, M. T. Sadiq, Z. Fan, and G. Xiao, "A new framework for automatic detection of motor and mental imagery EEG signals for robust BCI systems," *IEEE Trans. Instrum. Meas.*, vol. 70, pp. 1–12, 2021, doi: 10.1109/TIM.2021.3069026.

LU MA was born in Huaibei, Anhui, Han Nationality, in March 1979. He received the bachelor's degree in computer science and technology from Huaibei Normal University, in 2004, and the master's degree in software engineering from the University of Electronic Science and Technology of China, in 2015. He is currently pursuing the Ph.D. degree with the School of Information and Control Engineering, China University of Mining and Technology.

He has published three academic articles and two research projects. His main research interests include artificial intelligence, mathematical modeling, computer science and technology, and digital image processing.

HAIPENG XU was born in Henan, China, in 1982. He received the bachelor's degree from China University of Geosciences (Beijing), Beijing, China, and the master's degree from the University of the East, in 2023. He is currently pursuing the Ph.D. degree with Kyrgyz National University.

From 2006 to 2014, he was with Heilongjiang Construction Engineering Group. From 2014 to 2017, he was with Anyang Construction Engineering Group. Since 2017, he has been a Senior Engineer with Construction Management with Shangqiu City Development Investment Group Company Ltd. He has participated in one national project and four provincial projects, presided over and participated in ten project management, published more than five academic papers, and authorized more than six patents. His research interests include urban construction, project management, building digital modeling, optimization algorithms, regression analysis, and system optimization.